Computers and Mathematics with Applications 77 (2019) 1–14

Contents lists available at ScienceDirect

Computers and Mathematics with Applications

journal homepage: www.elsevier.com/locate/camwa

Quadrature for parabolic Galerkin BEM with moving surfaces☆

Nicole Manson, Johannes Tausch *

Department of Mathematics, Southern Methodist University, Dallas, TX 75275, USA

ARTICLE INFO

Article history:
Received 20 December 2017
Received in revised form 29 August 2018
Accepted 3 September 2018
Available online 27 September 2018

Keywords:
Boundary element method
Galerkin method
Moving geometry
Time dependent problem
Numerical quadrature
Error analysis

ABSTRACT

The successful implementation of the Galerkin Boundary Element Method hinges on the accurate and effective quadrature of the influence coefficients. For parabolic boundary integral operators quadrature must be performed in space and time where integrals have singularities when source- and evaluation points coincide. For problems where the surface is fixed, the time integration can be performed analytically, but for moving geometries numerical quadrature in space and time must be used. For this case a set of transformations is derived that render the singular space–time integrals into smooth integrals that can be treated with standard tensor product Gauss quadrature rules. This methodology can be applied to the heat equation and to transient Stokes flow.

1. Introduction

The boundary element method is a well known technique to solve parabolic boundary value problems which has generated considerable interest in engineering [1–3] as well as in the mathematics literature [4–7]. Time dependence is reflected in the fact that parabolic layer potential operators involve integrals over time in addition to the boundary surface. For instance, the single layer potential of the heat equation with the density $g(\cdot)$ on a boundary surface Γ is

$$\mathcal{V}g(\mathbf{x},t)=\int_0^t\int_\Gamma \frac{1}{\left(4\pi(t-\tau)\right)^{\frac{3}{2}}}\exp\left(-\frac{|\mathbf{x}-\mathbf{y}|^2}{4(t-\tau)}\right)g(\mathbf{y},\tau)\,ds(\mathbf{y})d\tau\,. \tag{1}$$

To accommodate more general parabolic equations and potentials we assume the kernel has the form

$$G(\mathbf{x},\mathbf{y},t-\tau)=\frac{1}{(t-\tau)^{\frac{n}{2}}}K\left(\boldsymbol{\rho},\mathbf{x},\mathbf{y}\right), \tag{2}$$

where

$$\boldsymbol{\rho}=\frac{\mathbf{x}-\mathbf{y}}{\sqrt{4(t-\tau)}}. \tag{3}$$

Here, n is a positive integer that reflects the singularity of the Green's function. Specific examples will be discussed in Section 6. Because of the causality of parabolic boundary operators we have $G=0$ whenever $t<\tau$.

We make the following assumptions about K. Later, we will show that they are satisfied for the potentials of the heat equation and transient Stokes flow.

☆ This material is based upon work supported by the National Science Foundation, USA, under grant DMS-1115931.
* Corresponding author.
E-mail addresses: ndeyerl@smu.edu (N. Manson), tausch@smu.edu (J. Tausch).

https://doi.org/10.1016/j.camwa.2018.09.004
0898-1221/

Assumption 1. The function K is C^∞ in all variables. Further, there is an integer M such that the function

$$(\mu, \boldsymbol{\rho}, \mathbf{x}, \mathbf{y}) \to \frac{1}{\mu^M} K\left(\frac{\boldsymbol{\rho}}{\mu}, \mathbf{x}, \mathbf{y}\right)$$

is C^∞ for $\mu \in [0, 1]$, $\boldsymbol{\rho} \neq \mathbf{0}$ and $\mathbf{x}, \mathbf{y} \in \mathbb{R}^3$.

Note that for M sufficiently large, the kernel G is singular only if $(\mathbf{y}, \tau) = (\mathbf{x}, t)$. There are several options for the discretization of parabolic boundary equations, they are surveyed in [8]. Here we focus on the Galerkin method, because of its effectiveness for non-smooth and time dependent geometries. These advantages come at a price, as the calculation of the influence coefficients of the discretized layer potentials involve complicated and possibly singular space–time integrals. To motivate the ensuing discussion, consider a time-dependent surface $\Gamma = \Gamma(t)$ which has been subdivided into a conforming triangulation with patches $\Gamma_p(t)$, $p = 1, \ldots, P$. To keep things manageable we assume that $\Gamma(t)$ and its triangulation are isomorphic to the initial surface and triangulation. Further, the time interval $I = [0, T]$ has been subdivided into equal subintervals $I_i = [ih_t, (i + 1)h_t]$ where h_t is the time step size. The test- and ansatz spaces consist of piecewise polynomials on this space–time subdivision.

To realize the Galerkin discretization integrals of the form

$$I^{i,j}_{p,q} = \int_{I_i} \int_{\Gamma_p(t)} \int_{I_j} \int_{\Gamma_q(\tau)} G(\mathbf{x}, \mathbf{y}, t - \tau)\phi^I(\tau)\phi^I(t)\,\phi^\Gamma(\mathbf{y})\phi^\Gamma(\mathbf{x})\, ds(\mathbf{y})d\tau\, ds(\mathbf{x})dt \tag{4}$$

must be computed, where $\phi^I, \phi^I, \phi^\Gamma, \phi^\Gamma$ are polynomial shape functions.

When the surface is stationary one can rearrange the order of integration such that the time variables appear inside of the space variables. For the heat kernel and the transient Stokeslet these time integrals can be expressed in closed form using incomplete gamma functions [9,10]. The result is a space-dependent kernel $G_{ij}(\mathbf{x}, \mathbf{y})$, that is smooth if the time intervals I_i and I_j are well-separated. Otherwise, if $j = i$ or $j = i - 1$ the functions or derivatives of $G_{ij}(\cdot)$ are singular for $\mathbf{x} = \mathbf{y}$. In these cases, the singularity removing transformations for elliptic boundary operators [11,12] are applicable to compute the integrals (4) by numerical quadrature, see [13,14].

Unfortunately, this trick is limited to stationary surfaces whereas in many applications of interest the geometry is time dependent. For instance, melting and solidification problems are governed by the heat equation and the objective is to determine the time dependent interface between the solid- and liquid phase, see e.g., [15,16]. Also problems governed by Stokes flow often involve moving surfaces, such as in Mems devices [17], micro-swimmers [18] and sedimentation [19].

The technical difficulty of moving geometries is that all variables in (4) must be handled by numerical quadrature. Because of the singularity new transformations in space–time must be derived, this is the goal of this work. One should note here that the papers [20,21] also deal with singularity removing transformation that can be seen as an extension of the construction in [11,12] to higher dimensions. However, the mentioned papers address elliptic operators. Because of the space–time scaling expressed by the variable $\boldsymbol{\rho}$ in the kernel of (2), the parabolic case is different and we did not see an obvious way to apply the earlier work to the case considered here.

The outline of the remainder of this paper is as follows. In Section 2 we will state some minimal assumptions on the geometry which ensure that the transformed integrals have indeed smooth integrands. Our construction has three stages, we first apply a transformation for the spatial variable (Section 3), followed by a transformation in time (Section 4). Since these two transformations still result in singular integrands we will then apply the Duffy transform in Section 5 to obtain a regular integrand. Note that Section 3 follows closely the discussion in [12] where a set of suitable transformations for elliptic boundary integral operators are derived. However, we felt that it was necessary to include this here at the expense of some repetition, in order to set the stage for the new contributions and to improve self consistency and readability of this work. We conclude in Section 7 with an illustration of the Galerkin BEM for parabolic moving boundary problems.

2. The setting

We consider the boundary surface of a time-dependent finite domain $\Gamma(t) = \partial\Omega(t)$ in three dimensions which is subdivided into a triangulation

$$\Gamma(t) = \bigcup_{p=1}^{P} \Gamma_p(t), \tag{5}$$

where each $\Gamma_p(t)$ is a parametric image of the unit triangle,

$$\sigma^{(2)} = \left\{\hat{\mathbf{x}} \in \mathbb{R}^2 \,:\, 0 \le \hat{x}_2 \le \hat{x}_1 \le 1\right\},$$

i.e.,

$$\Gamma_p(t) = \left\{\mathbf{x}_p(\hat{\mathbf{x}}, t),\ \hat{\mathbf{x}} \in \sigma^{(2)}\right\}.$$

The parametric images of the points $(0, 0)$, $(0, 1)$ and $(1, 1)$ are the vertices of the triangulation and the parametric images of the line segments $(\xi, 0)$, $(1, \xi)$ and (ξ, ξ), $\xi \in [0, 1]$ are the edges.

When considering a pair of patches $\Gamma_p(t)$ and $\Gamma_q(t)$ with a common vertex, then without loss of generality the common vertex can be assumed to be the parametric image of the origin $(0, 0) \in \sigma^{(2)}$. Otherwise, we can take the affine transformations S_p and S_q of $\sigma^{(2)}$ that map the common vertex into the origin and consider the parameterizations $\mathbf{x}_p \circ S_p$ and $\mathbf{x}_q \circ S_q$. With such a transformation it is also possible to parameterize a common edge by the line segment $(\xi, 0)$, $\xi \in [0, 1]$.

We make the following assumptions on the triangulation and the parameterizations.

Assumption 2.

1. The triangulation is time conforming in the sense that for all $t \in I$ the intersection of two different triangular patches $\Gamma_p(t) \cap \Gamma_q(t)$ is either empty, a common vertex or a common edge. Moreover, if two patches intersect for some $t \in I$, they intersect for all $t \in I$ in the same vertex or edge. The vertices and edges may, of course, move in time.
2. $\mathbf{x}_p \in C^\infty(\sigma^{(2)} \times I)$ and there are constants $C, c > 0$ such that
$$\begin{aligned}\left|\mathbf{x}_p(\hat{\mathbf{x}}, t) - \mathbf{x}_p(\hat{\mathbf{y}}, t)\right| &\geq c h_s \left|\hat{\mathbf{x}} - \hat{\mathbf{y}}\right|,\\ \left|\mathbf{x}_p(\hat{\mathbf{x}}, t) - \mathbf{x}_p(\hat{\mathbf{y}}, \tau)\right| &\leq C\left(h_s\left|\hat{\mathbf{x}} - \hat{\mathbf{y}}\right| + |t - \tau|\right).\end{aligned}$$
Here h_s is the maximal diameter of $\Gamma_p(t)$.
3. If $\Gamma_p(t)$ and $\Gamma_q(t)$ intersect in a common vertex or edge, then they satisfy the cone condition stated below in Definition 1.
4. If $\Gamma_p(t)$ and $\Gamma_q(t)$ intersect in a common edge, then $\mathbf{x}_p(\xi, 0, t) = \mathbf{x}_q(\xi, 0, t)$, $\xi \in [0, 1]$.

Definition 1.

1. If $\Gamma_p(t)$ and $\Gamma_q(t)$ have one common vertex $\mathbf{v}_0$, then they satisfy the cone condition if there is a $\gamma \in (0, 1)$ such that for all $\mathbf{x} \in \Gamma_p$ and $\mathbf{y} \in \Gamma_q$ and $t \in I$
$$(\mathbf{x} - \mathbf{v}_0) \cdot (\mathbf{y} - \mathbf{v}_0) \leq (1 - \gamma)|\mathbf{x} - \mathbf{v}_0||\mathbf{y} - \mathbf{v}_0|$$
holds.
2. If Γ_p and Γ_q have a common edge then for $\mathbf{x} = \mathbf{x}_p(\hat{\mathbf{x}}, t) \in \Gamma_p$ the point $\mathbf{v}_x = \mathbf{x}_p(\hat{x}_1, 0, t)$ is the projection of $\mathbf{x}$ on the common edge. Further, the two panels satisfy the cone condition if there is a $\gamma > 0$ such that for all $\mathbf{x} \in \Gamma_p$, $\mathbf{y} \in \Gamma_q$ and $t \in I$
$$(\mathbf{x} - \mathbf{v}_x) \cdot (\mathbf{y} - \mathbf{v}_x) \leq (1 - \gamma)|\mathbf{x} - \mathbf{v}_x||\mathbf{y} - \mathbf{v}_x|$$
holds.

The first cone condition states that for every $\mathbf{x} \in \Gamma_p$ there is a cone with vertex $\mathbf{v}_0$ and axis in direction of $\mathbf{x} - \mathbf{v}_0$ such that Γ_q intersects with this cone only in $\mathbf{v}_0$. Similarly, the second condition states that there is a cone with vertex $\mathbf{v}_x$ and axis in direction of $\mathbf{x} - \mathbf{v}_x$ such that Γ_q intersects with this cone only in $\mathbf{v}_x$. Since p and q are interchangeable, a similar condition holds for $\mathbf{y}$, $\mathbf{v}_y$ and Γ_p.

If $\mathbf{x} \in \Gamma_p$, $\mathbf{y} \in \Gamma_q$ and $\mathbf{v}$ is either $\mathbf{v}_0$ or $\mathbf{v}_x$ or $\mathbf{v}_y$ in either cone condition, then the computation
$$\begin{aligned}|\mathbf{x} - \mathbf{y}|^2 &= |\mathbf{x} - \mathbf{v}|^2 + |\mathbf{y} - \mathbf{v}|^2 - 2(\mathbf{x} - \mathbf{v}) \cdot (\mathbf{y} - \mathbf{v})\\ &\geq |\mathbf{x} - \mathbf{v}|^2 + |\mathbf{y} - \mathbf{v}|^2 - 2(1 - \gamma)|\mathbf{x} - \mathbf{v}||\mathbf{y} - \mathbf{v}|\\ &\geq |\mathbf{x} - \mathbf{v}|^2 + |\mathbf{y} - \mathbf{v}|^2 - (1 - \gamma)\left(|\mathbf{x} - \mathbf{v}|^2 + |\mathbf{y} - \mathbf{v}|^2\right)\\ &= \gamma\left(|\mathbf{x} - \mathbf{v}|^2 + |\mathbf{y} - \mathbf{v}|^2\right)\end{aligned}$$
implies the inequality
$$|\mathbf{x} - \mathbf{y}| \geq \alpha\left(|\mathbf{x} - \mathbf{v}| + |\mathbf{y} - \mathbf{v}|\right) \tag{6}$$
with $\alpha = \sqrt{\gamma/2}$.

There are many practical situations where Assumption 2 can be satisfied. This includes rigid motions or geometries that grow or shrink without the need of mesh refinements. To illustrate these ideas, consider a time conforming triangulation where all patches are flat. If the vertices of Γ_p are $\mathbf{v}_0, \mathbf{v}_1, \mathbf{v}_2$ then an obvious parameterization is
$$\mathbf{x}_p(\hat{\mathbf{x}}, t) = \mathbf{v}_0(t) + \hat{x}_1\mathbf{a}_1(t) + \hat{x}_2\mathbf{a}_2(t)$$
where $\mathbf{a}_1(t) = \mathbf{v}_1(t) - \mathbf{v}_0(t)$, $\mathbf{a}_2(t) = \mathbf{v}_2(t) - \mathbf{v}_1(t)$ are two of the three edges.

If all interior angles are positive, then Assumption 2. 2. is obviously satisfied. Further, if the angle between adjacent panels remains positive for all times, then the cone conditions are also satisfied. Note that for a flat triangle, the vector $\mathbf{x} - \mathbf{v}_\mathbf{x}$ is parallel to $\mathbf{a}_2$, see Fig. 1.

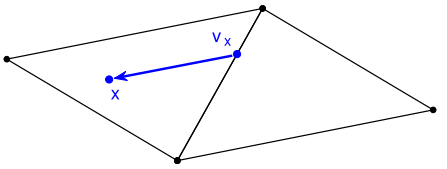

Fig. 1. A pair of triangles with a common edge and the projection $\mathbf{v}_x$ of a point $\mathbf{x}$.

Below, we will frequently use the following fact which follows from standard calculus of multivariate functions.

Lemma 1. *If $D \subset \mathbb{R}^d$ is convex and $\mathbf{f}$ is a smooth and possibly vector valued function in D, then there are smooth functions $\mathbf{a}_k$ such that for $\mathbf{z}, \mathbf{w} \in D$*

$$\mathbf{f}(\mathbf{z}) - \mathbf{f}(\mathbf{w}) = \sum_{k=1}^{d} \mathbf{a}_k(\mathbf{z}, \mathbf{w})(z_k - w_k)$$

holds.

We make the following observations about patches with nonempty intersections in a time dependent triangulation that satisfies Assumption 2.

Self panel, $p = q$.

Assumption 2. 2. states that

$$\left|\mathbf{x}_p(\hat{\mathbf{x}}, t) - \mathbf{x}_p(\hat{\mathbf{y}}, t)\right| \geq ch_s\left|\hat{\mathbf{x}} - \hat{\mathbf{y}}\right|. \tag{7}$$

Further, by setting $\mathbf{z} = (\hat{\mathbf{x}}, t)$, $\mathbf{w} = (\hat{\mathbf{y}}, \tau)$ and $\mathbf{f} = \mathbf{x}_p$ it follows from Lemma 1 that there are smooth functions $\mathbf{a}_1 = \mathbf{a}_1(\hat{\mathbf{x}}, \hat{\mathbf{y}}, t, \tau)$, $\mathbf{a}_2 = \mathbf{a}_2(\hat{\mathbf{x}}, \hat{\mathbf{y}}, t, \tau)$ and $\mathbf{v} = \mathbf{v}(\hat{\mathbf{x}}, \hat{\mathbf{y}}, t, \tau)$ such that

$$\mathbf{x}_p(\hat{\mathbf{x}}, t) - \mathbf{x}_p(\hat{\mathbf{y}}, \tau) = \mathbf{a}_1(\hat{x}_1 - \hat{y}_1) + \mathbf{a}_2(\hat{x}_2 - \hat{y}_2) + \mathbf{v}(t - \tau) \tag{8}$$

To make our notations less cluttered we omit the dependence of the vectors $\mathbf{a}_1$, $\mathbf{a}_2$ and $\mathbf{v}$ on the variables $\hat{\mathbf{x}}$, $\hat{\mathbf{y}}$, t and τ.

Common edge.

If Γ_p and Γ_q have a common edge then it follows from applying (6) two times, that

$$\begin{aligned}
&\left|\mathbf{x}_p(\hat{\mathbf{x}}, t) - \mathbf{x}_q(\hat{\mathbf{y}}, t)\right| \\
&\quad \geq \alpha\left(\left|\mathbf{x}_p(\hat{\mathbf{x}}, t) - \mathbf{x}_p(\hat{x}_1, 0, t)\right| + \left|\mathbf{x}_p(\hat{x}_1, 0, t) - \mathbf{x}_q(\hat{\mathbf{y}}, t)\right|\right) \\
&\quad \geq \alpha^2\left(\left|\mathbf{x}_p(\hat{\mathbf{x}}, t) - \mathbf{x}_p(\hat{x}_1, 0, t)\right| + \left|\mathbf{x}_p(\hat{x}_1, 0, t) - \mathbf{x}_q(\hat{y}_1, 0, t)\right| + \left|\mathbf{x}_q(\hat{y}_1, 0, t) - \mathbf{x}_q(\hat{\mathbf{y}}, t)\right|\right)
\end{aligned}$$

and thus it follows from Assumption 2. 4. and estimate (7) that there is a constant $c > 0$ such that

$$\left|\mathbf{x}_p(\hat{\mathbf{x}}, t) - \mathbf{x}_q(\hat{\mathbf{y}}, t)\right| \geq ch_s\left(\left|\hat{x}_1 - \hat{y}_1\right| + \hat{x}_2 + \hat{y}_2\right). \tag{9}$$

If, in Lemma 1, we let $\mathbf{z} = (\hat{\mathbf{x}}, \hat{\mathbf{y}}, t, \tau)$, $\mathbf{w} = (\hat{y}_1, 0, \hat{y}_1, 0, \tau, \tau)$ and $\mathbf{f}(\mathbf{z}) = \mathbf{x}_p(\hat{\mathbf{x}}, t) - \mathbf{x}_q(\hat{\mathbf{y}}, \tau)$ then $\mathbf{f}(\mathbf{w}) = \mathbf{x}_p(\hat{y}_1, 0, \tau) - \mathbf{x}_q(\hat{y}_1, 0, \tau) = \mathbf{0}$ and thus there are smooth functions $\mathbf{a}_1, \ldots, \mathbf{a}_3$ and $\mathbf{v}$, such that

$$\mathbf{x}_p(\hat{\mathbf{x}}, t) - \mathbf{x}_q(\hat{\mathbf{y}}, \tau) = \mathbf{a}_1(\hat{x}_1 - \hat{y}_1) + \mathbf{a}_2\hat{x}_2 + \mathbf{a}_3\hat{y}_2 + \mathbf{v}(t - \tau). \tag{10}$$

Common vertex.

If Γ_p and Γ_q have exactly one common vertex then

$$\left|\mathbf{x}_p(\hat{\mathbf{x}}, t) - \mathbf{x}_q(\hat{\mathbf{y}}, t)\right| \geq ch_s\left(\hat{x}_1 + \hat{x}_2 + \hat{y}_1 + \hat{y}_2\right). \tag{11}$$

which can be derived from the cone condition using similar arguments as before.

If we let $\mathbf{z} = (\hat{\mathbf{x}}, \hat{\mathbf{y}}, t, \tau)$, $\mathbf{w} = (\mathbf{0}, \mathbf{0}, \tau, \tau)$ and $\mathbf{f}(\mathbf{z}) = \mathbf{x}_p(\hat{\mathbf{x}}, t) - \mathbf{x}_q(\hat{\mathbf{y}}, \tau)$ then $\mathbf{f}(\mathbf{w}) = \mathbf{x}_p(\mathbf{0}, \tau) - \mathbf{x}_q(\mathbf{0}, \tau) = \mathbf{0}$ and thus it follows from Lemma 1 that there are smooth functions $\mathbf{a}_1, \ldots, \mathbf{a}_4$ and $\mathbf{v}$, such that

$$\mathbf{x}_p(\hat{\mathbf{x}}, t) - \mathbf{x}_q(\hat{\mathbf{y}}, \tau) = \mathbf{a}_1\hat{x}_1 + \mathbf{a}_2\hat{x}_2 + \mathbf{a}_3\hat{y}_1 + \mathbf{a}_4\hat{y}_2 + (t - \tau)\mathbf{v}. \tag{12}$$

3. Spatial transformations

It will become apparent in Section 5 that space and time can be treated separately when designing singularity removing transformations. In this section we begin with suitable transformations for the spatial variables $\hat{\mathbf{x}}$ and $\hat{\mathbf{y}}$ in (4). They are

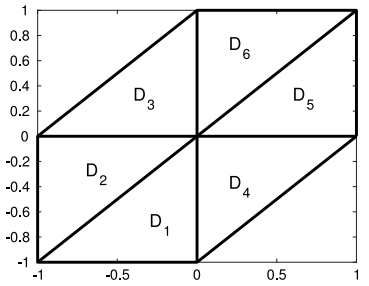

Fig. 2. Domain of z-integration for the self panel case.

designed to handle singularities of the integrand when $\mathbf{x} = \mathbf{y}$, which can happen when Γ_p and Γ_q are either the same patch, or patches with a common edge or vertex. This parallels the construction for elliptic integral operators. We recall this here for completeness, following the discussion in [12] closely.

Self panel, $p = q$.

Since the integrand is singular when $\hat{\mathbf{x}} = \hat{\mathbf{y}}$, we introduce the transformation

$$\begin{aligned} z_1 &= \hat{y}_1 - \hat{x}_1 & \hat{x}_1 &= w_1 \\ z_2 &= \hat{y}_2 - \hat{x}_2 & \hat{x}_2 &= w_2 \\ w_1 &= \hat{x}_1 & \hat{y}_1 &= z_1 + w_1 \\ w_2 &= \hat{x}_2 & \hat{y}_2 &= z_2 + w_2 \end{aligned} \tag{13}$$

For $\hat{\mathbf{x}}, \hat{\mathbf{y}}$ in $\sigma^{(2)}$ it is easy to see that the $\mathbf{z} = (z_1, z_2)$-variables must be in the union of six triangles

$$\begin{bmatrix} z_1 \\ z_2 \end{bmatrix} \in D_1 \cup \cdots \cup D_6,$$

see Fig. 2. Each triangle D_k can be mapped on the unit square with the Duffy transform. Thus

$$\mathbf{z} = \xi \mathbf{r}_\mathbf{k}(\eta_1), \quad \mathbf{z} \in D_k, \quad (\xi, \eta_1) \in [0, 1]^2, \tag{14}$$

for $k \in \{1, \ldots, 6\}$. The domain of integration of the $\mathbf{w} = (w_1, w_2)$-variables depends on $\mathbf{z}$. From (13) it follows that

$$W_k(\mathbf{z}) = \sigma^{(2)} \cap \left(-\mathbf{z} + \sigma^{(2)}\right)$$

Since $W_k(\mathbf{z})$ is the intersection of $\sigma^{(2)}$ with a shifted version of $\sigma^{(2)}$ it is an axiparallel isosceles right triangle with side length $1 - \xi$. Thus the transformation that maps the unit square to $W_k(\mathbf{z})$ is

$$\mathbf{w} = \mathbf{v}_\mathbf{k} + (1 - \xi) \begin{bmatrix} \eta_2 \\ \eta_2 \eta_3 \end{bmatrix}, \quad (\eta_2, \eta_3) \in [0, 1]^2.$$

where $\mathbf{v}_k$ is the lower left corner. For the six subdomains we thus obtain

$$\begin{aligned} k = 1: &\quad \mathbf{r}_1 = \begin{bmatrix} -\eta_1 \\ -1 \end{bmatrix} & \mathbf{v}_1 &= \begin{bmatrix} \xi \\ \xi \end{bmatrix} \\ k = 2: &\quad \mathbf{r}_2 = \begin{bmatrix} -1 \\ -\eta_1 \end{bmatrix} & \mathbf{v}_2 &= \begin{bmatrix} \xi \\ \xi \eta_1 \end{bmatrix} \\ k = 3: &\quad \mathbf{r}_3 = \begin{bmatrix} -\eta_1 \\ 1 - \eta_1 \end{bmatrix} & \mathbf{v}_3 &= \begin{bmatrix} \xi \\ 0 \end{bmatrix} \\ k = 4: &\quad \mathbf{r}_4 = \begin{bmatrix} 1 - \eta_1 \\ -\eta_1 \end{bmatrix} & \mathbf{v}_4 &= \begin{bmatrix} \xi \eta_1 \\ \xi \eta_1 \end{bmatrix} \\ k = 5: &\quad \mathbf{r}_5 = \begin{bmatrix} 1 \\ \eta_1 \end{bmatrix} & \mathbf{v}_5 &= \begin{bmatrix} 0 \\ 0 \end{bmatrix} \\ k = 6: &\quad \mathbf{r}_6 = \begin{bmatrix} \eta_1 \\ 1 \end{bmatrix} & \mathbf{v}_6 &= \begin{bmatrix} \xi(1 - \eta_1) \\ 0 \end{bmatrix} \end{aligned} \tag{15}$$

In all cases the Jacobian of the transformation is $J = \xi(1 - \xi)^2 \eta_2$.

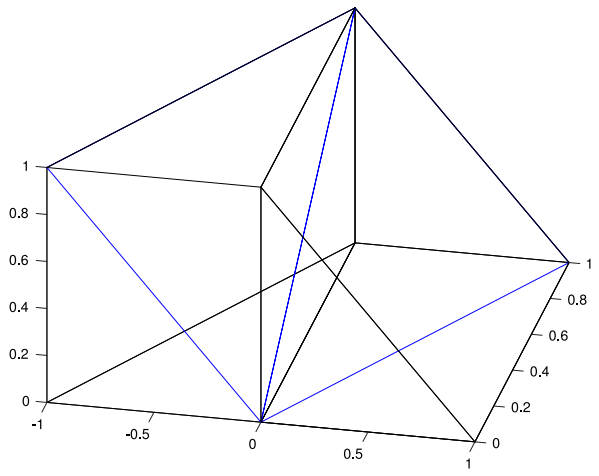

Fig. 3. Domain of z-integration for the case of a common edge.

Common edge.

In this case we introduce the transformation

$$\begin{aligned} z_1 &= \hat{y}_1 - \hat{x}_1 & \hat{x}_1 &= w_1 \\ z_2 &= \hat{y}_2 & \hat{x}_2 &= z_3 \\ z_3 &= \hat{x}_2 & \hat{y}_1 &= z_1 + w_1 \\ w_1 &= \hat{x}_1 & \hat{y}_2 &= z_2 \end{aligned} \tag{16}$$

For $\hat{\mathbf{x}}, \hat{\mathbf{y}}$ in $\sigma^{(2)}$ it is easy to see that the $\mathbf{z} = (z_1, z_2, z_3)$-variables must be in the union of four polyhedra $D_1 \cup D_2 \cup D_3 \cup D_4$, which have one vertex in the origin and are characterized by the opposite face, see Fig. 3.

Thus we write

$$\mathbf{z} = \xi \mathbf{r}_{\mathbf{k}}(\eta_1, \eta_2), \quad \mathbf{z} \in D_k, \quad (\xi, \eta_1, \eta_2) \in [0, 1]^3, \tag{17}$$

for $k \in \{1, \ldots, 4\}$, where $\mathbf{r}_k(\eta_1, \eta_2)$ parameterizes the opposite face. Moreover, it follows from (16) that w_1 must be in the intersection $w_1 \in [-z_1, 1 - z_1] \cap [0, 1]$.

$$\begin{aligned} k = 1: \quad \mathbf{r}_1 &= \begin{bmatrix} -\eta_1 \\ 1 - \eta_1 \\ \eta_2 \end{bmatrix} & w_1 &= \xi + (1 - \xi)\eta_3 & J_1 &= (1 - \xi)\xi^2 \\ k = 2: \quad \mathbf{r}_2 &= \begin{bmatrix} -\eta_1\eta_2 \\ (1 - \eta_1)\eta_2 \\ 1 \end{bmatrix} & w_1 &= \xi + (1 - \xi)\eta_3 & J_2 &= (1 - \xi)\xi^2\eta_2 \\ k = 3: \quad \mathbf{r}_3 &= \begin{bmatrix} 1 - \eta_1 \\ \eta_2 \\ \eta_1 \end{bmatrix} & w_1 &= (1 - \eta_1)\xi + (1 - \xi)\eta_3 & J_3 &= (1 - \xi)\xi^2 \\ k = 4: \quad \mathbf{r}_4 &= \begin{bmatrix} \eta_1\eta_2 \\ 1 \\ (1 - \eta_1)\eta_2 \end{bmatrix} & w_1 &= \xi(1 - \eta_1\eta_2) + (1 - \xi)\eta_3 & J_4 &= (1 - \xi)\xi^2\eta_2 \end{aligned} \tag{18}$$

Common vertex.

In this case the transformation is simply

$$\begin{aligned} z_1 &= \hat{x}_1 \\ z_2 &= \hat{x}_2 \\ z_3 &= \hat{y}_2 \\ z_4 &= \hat{y}_1 \end{aligned}$$

The $\mathbf{z}$-domain can be split into two regions $\sigma^{(2)} \otimes \sigma^{(2)} = D_1 \cup D_2$, where

$$D_1 = \left\{ \mathbf{z} \ : \ \begin{array}{c} 0 \le z_2 \le z_1 \le 1 \\ 0 \le z_4 \le z_3 \le 1 \\ z_3 \le z_1 \end{array} \right\}, \text{ and } D_2 = \left\{ \mathbf{z} \ : \ \begin{array}{c} 0 \le z_2 \le z_1 \le 1 \\ 0 \le z_4 \le z_3 \le 1 \\ z_1 \le z_3 \end{array} \right\}.$$

Thus

$$\mathbf{z} = \xi \mathbf{r}_{\mathbf{k}}(\eta_1, \eta_2, \eta_3), \quad \mathbf{z} \in D_k, \quad \xi, \eta_1, \eta_2 \in [0, 1]^3, \tag{19}$$

where

$$\mathbf{r}_1 = \begin{bmatrix} 1 \\ \eta_1 \\ \eta_2 \\ \eta_2\eta_3 \end{bmatrix} \text{ and } \mathbf{r}_2 = \begin{bmatrix} \eta_2 \\ \eta_2\eta_3 \\ 1 \\ \eta_1 \end{bmatrix}. \tag{20}$$

In both cases the Jacobian is $J = \xi^3\eta_2$.

4. Temporal transformations

We now single out the time integration in the integrals of the type (4). To that end, we start with a transformation for a singular time integral

$$I_0 = \int_{t_i}^{t_{i+1}} \int_{t_i}^{t} \frac{f(t, \tau)}{(t-\tau)^{\frac{n}{2}}} \, d\tau dt$$

where f is a smooth function. The transformation

$$\begin{array}{ll} \zeta = \sqrt{(t-\tau)/h_t}, & t = h_t(\zeta^2 + \omega) + t_i, \\ \omega = (\tau - t_i)/h_t, & \tau = h_t\omega + t_i, \end{array} \tag{21}$$

has Jacobian $J = 2h_t^2\zeta$. This transformation maps the triangular (t, τ)-integration domain to $\{(\zeta, \omega) : 0 \le \omega \le 1 - \zeta^2, \ 0 \le \zeta \le 1\}$. In the second step we transform the ω-variable

$$\omega = (1 - \zeta^2)\eta_4$$

which gives a unit square in the (ζ, η_4)-plane. Thus

$$I_0 = 2h_t^{2-\frac{n}{2}} \int_0^1 \int_0^1 \zeta^{1-n} \widetilde{f}(\zeta, \eta_4) \, d\zeta d\eta_4,$$

where $\widetilde{f}$ is a smooth function that incorporates the Jacobian from the η_4-transformation. The integrand is smooth as long as $n \le 1$.

In the case $j = i - 1$ the singularity occurs only at one point $t = \tau = t_i$, thus we split the integral into two triangular regions

$$I_1 = \int_{t_i}^{t_{i+1}} \int_{t_{i-1}}^{t_i} \frac{f(t, \tau)}{(t-\tau)^{\frac{n}{2}}} \, d\tau dt = \int_{t_i}^{t_{i+1}} \int_{t_{i-1}}^{t-h_t} \frac{f(t, \tau)}{(t-\tau)^{\frac{n}{2}}} \, d\tau dt + \int_{t_i}^{t_{i+1}} \int_{t-h_t}^{t_i} \frac{f(t, \tau)}{(t-\tau)^{\frac{n}{2}}} \, d\tau dt.$$

The first integral can be treated by standard means and the second integral (denoted by I_1^+) contains the singularity. To derive the transformation for the second integral consider the transformation

$$\begin{array}{ll} \zeta = \sqrt{(t-\tau)/h_t}, & t = h_t(\zeta^2 - \omega) + t_i, \\ \omega = (t_i - \tau)/h_\tau, & \tau = t_i - h_\tau\omega, \end{array} \tag{22}$$

which has Jacobian $J = 2h_t h_\tau \zeta$. This transformation maps the triangle in the (t, τ) plane to the domain $\{(\zeta, \omega) : 0 \le \omega \le \zeta^2, \ 0 \le \zeta \le 1\}$. In the second step we transform the ω-variable

$$\omega = \zeta^2\eta_4$$

which gives a unit square in the (ζ, η_4)-plane. Thus

$$I_1^+ = 2h_t^{2-\frac{n}{2}} \int_0^1 \int_0^1 \zeta^{3-n} \widetilde{f}(\zeta, \eta_4) \, d\zeta d\eta_4$$

has a smooth integrand as long as $n \le 3$.

5. Combining space and time transformations

We now turn to the type of integrals that have to be computed in the implementation of the Galerkin boundary element method of parabolic problems. In the parameterization of Section 2 the integral (4) appears as

$$I_{p,q}^{i,j} = \int_{t_i}^{t_{i+1}} \int_{t_j}^{t_{j+1}} \int_{\sigma^{(2)}} \int_{\sigma^{(2)}} \frac{1}{(t-\tau)^{\frac{n}{2}}} K(\boldsymbol{\rho}, \mathbf{x}, \mathbf{y})\, \hat{\Phi}(\hat{\mathbf{x}}, \hat{\mathbf{y}}, t, \tau)\, d^2\hat{\mathbf{x}}\, d^2\hat{\mathbf{y}} d\tau dt. \tag{23}$$

where $\boldsymbol{\rho}$, $\mathbf{x}$ and $\mathbf{y}$ are now considered functions of $\hat{\mathbf{x}}$ and $\hat{\mathbf{y}}$ and the smooth function $\hat{\Phi}$ incorporates all shape functions and Jacobians of surface parameterizations.

This integral is singular only if $j = i$ or $j = i-1$ and if the panels are identical or have a common edge or vertex. Together with the temporal transforms (21) or (22) we obtain from (23) either six, four or two integrals of the type

$$I = \int_0^1 \int_0^1 \int_{[0,1]^4} \frac{\xi^m}{\zeta^{n-1}} K(\boldsymbol{\rho}, \mathbf{x}, \mathbf{y}) \widetilde{\Phi}(\xi, \zeta, \boldsymbol{\eta}) d^4\boldsymbol{\eta}\, d\xi d\zeta, \tag{24}$$

where ξ^m, $m \in \{1, 2, 3\}$ comes from the Jacobian in the spatial transformations, $\widetilde{\Phi}$ is the function Φ in the transformed coordinates and also contains Jacobians and $\boldsymbol{\rho}$, $\mathbf{x}$, $\mathbf{y}$ are functions of the new variables.

Integral (24) is still singular. To regularize it split the unit square in the (ξ, ζ)-plane into two triangles and apply the Duffy transforms

$$\begin{bmatrix} \xi \\ \zeta \end{bmatrix} = \lambda \begin{bmatrix} 1 \\ \mu \end{bmatrix} \quad \text{and} \quad \begin{bmatrix} \xi \\ \zeta \end{bmatrix} = \lambda \begin{bmatrix} \mu \\ 1 \end{bmatrix}. \tag{25}$$

The Jacobians contribute an extra factor of λ. This results in two integrals $I = I_a + I_b$, where

$$I_a = \int_0^1 \int_0^1 \int_{[0,1]^4} \frac{\lambda^{2+m-n}}{\mu^{n-1}} K(\boldsymbol{\rho}, \mathbf{x}, \mathbf{y}) \Phi(\lambda, \mu, \boldsymbol{\eta}) d^4\boldsymbol{\eta}\, d\lambda d\mu, \tag{26}$$

$$I_b = \int_0^1 \int_0^1 \int_{[0,1]^4} \lambda^{2+m-n} \mu^m K(\boldsymbol{\rho}, \mathbf{x}, \mathbf{y}) \Phi(\lambda, \mu, \boldsymbol{\eta}) d^4\boldsymbol{\eta}\, d\lambda d\mu. \tag{27}$$

In the remainder of this section we show that I_a and I_b are regular integrals and therefore standard rules can be used for their quadrature. In all singular cases, it follows from (8), (10), (12), and the discussion in Section 3 that

$$\mathbf{x} - \mathbf{y} = \xi A\mathbf{r} + (t-\tau)\mathbf{v}. \tag{28}$$

where $A = A(\xi, \boldsymbol{\eta}, t, \tau) \in \mathbb{R}^{3\times 2}$ is a matrix, and $\mathbf{r} = \mathbf{r}(\boldsymbol{\eta})$ is the vector defined in (14),(17) and (19), respectively.

Lemma 2. *There are constants $c > 0$, $\tau_0 > 0$ such that for $(t, \tau) \in \sigma^{(2)}$ with $\tau \geq t - \tau_0$ the estimate*

$$|A\mathbf{r}| \geq \frac{c}{2} h_s \tag{29}$$

holds.

Proof. First consider the case $t = \tau$. It follows from (7), (9), (11) and going through the transformations in Section 3 that

$$|\mathbf{x} - \mathbf{y}| \geq c h_s |\mathbf{z}| = c h_s \xi |\mathbf{r}|. \tag{30}$$

Recall that in all singular cases (15) (18) and (20) $\mathbf{r} = \mathbf{r}(\boldsymbol{\eta})$ parameterizes a side of the $\mathbf{z}$-domain that is opposite to the origin. Hence the vector $\mathbf{r}$ is always non-zero, in fact, it can be found that $|\mathbf{r}| \geq 1/\sqrt{2}$. Moreover, because of $t = \tau$ Eq. (28) simplifies to

$$\mathbf{x} - \mathbf{y} = \xi A\mathbf{r}. \tag{31}$$

Combining (30) and (31) gives

$$|A\mathbf{r}| \geq \frac{c}{\sqrt{2}} h_s \tag{32}$$

which holds for $A = A(\xi, \boldsymbol{\eta}, t, t)$. By continuity of A, we can conclude that for some $\tau_0 > 0$ and a smaller constant on the right hand side, the above inequality also holds for τ when $t - \tau_0 \leq \tau \leq t$. This is the assertion.

Theorem 1. *If $2 + m - n \geq 0$ and $n \leq M + 1$ then the integrands of I_a and I_b are C^∞ in all variables.*

Proof. First consider $\boldsymbol{\rho}$ in the transformed variables. We have

$$\boldsymbol{\rho} = \frac{\mathbf{x} - \mathbf{y}}{\sqrt{4(t-\tau)}} = \frac{\xi}{\zeta} \frac{A\mathbf{r}}{\sqrt{4h_t}} + \zeta \frac{\sqrt{h_t}}{2} \mathbf{v} = \frac{\xi}{\zeta} \widetilde{\boldsymbol{\rho}},$$

where $\widetilde{\boldsymbol{\rho}}$ is a smooth function of ξ, ζ and $\boldsymbol{\eta}$. In the second transform of (25) we have $\xi/\zeta = \mu$ and therefore $\boldsymbol{\rho}$ is a smooth function of $(\mu, \lambda, \boldsymbol{\eta})$ and so is the integrand of I_b.

In the first transform of (25) we have $\xi/\zeta = 1/\mu$ so the limit $\mu \to 0$ must be considered more carefully. Since $\mu = 0$ corresponds to $t = \tau$ it follows from Lemma 2 that for small values of μ

$$|\widetilde{\boldsymbol{\rho}}| = \left| \frac{A\mathbf{r}}{\sqrt{4h_t}} + \zeta\mu\frac{h_t}{2}\mathbf{v} \right| \geq c\frac{h_s}{\sqrt{h_t}}$$

is uniformly bounded away from zero. Therefore Assumption 1 implies that the integrand in (26) is smooth for the given range of n and the proof is complete.

6. Examples of kernels

In this section we verify that Assumption 1 of Theorem 1 is indeed satisfied for the typical layer potentials of the Heat equation and transient Stokes flow.

Single layer heat kernel

The function K in (2) that corresponds to the single layer operator of the heat equation is

$$K(\boldsymbol{\rho}, \mathbf{x}, \mathbf{y}) = \exp\left(-|\boldsymbol{\rho}|^2\right)$$

with $n = 3$. Assumption 1 is satisfied for any positive integer M and thus the transformations discussed in the previous sections will lead to a regular integral.

Double layer heat kernel

For the double layer operator we have to consider the quantity $(\mathbf{x} - \mathbf{y}) \cdot \mathbf{n}_\mathbf{y}$. From standard calculus of surface parameterizations, it can be concluded that there is a matrix $B = B(\hat{\mathbf{x}}, \hat{\mathbf{y}}, \tau)$, a vector $\mathbf{b} = \mathbf{b}(\hat{\mathbf{x}}, \hat{\mathbf{y}}, \tau)$ and a scalar $\beta = \beta(\hat{\mathbf{y}}, t, \tau)$ such that for $\mathbf{x} \in \Gamma_p$ and $\mathbf{y} \in \Gamma_q$

$$(\mathbf{x} - \mathbf{y}) \cdot \mathbf{n}_\mathbf{y} = \begin{cases} (\hat{\mathbf{x}} - \hat{\mathbf{y}})^T B(\hat{\mathbf{x}} - \hat{\mathbf{y}}) + \beta(t - \tau) & \text{if } \Gamma_p = \Gamma_q, \\ \mathbf{b}^T(\hat{\mathbf{x}} - \hat{\mathbf{y}}) + \beta(t - \tau) & \Gamma_p,\ \Gamma_q \text{ have a common vertex or edge.} \end{cases}$$

With the transformations of Sections 3 to 5 it follows that there are scalar functions $\widetilde{b} = \widetilde{b}(\xi, \zeta, \boldsymbol{\eta})$ and $\widetilde{\beta} = \widetilde{\beta}(\xi, \zeta, \boldsymbol{\eta})$ such that

$$\frac{(\mathbf{x} - \mathbf{y}) \cdot \mathbf{n}_\mathbf{y}}{2(t - \tau)} = \begin{cases} \left(\frac{\xi}{\zeta}\right)^2 \widetilde{b} + \widetilde{\beta} & \text{if } \Gamma_p = \Gamma_q, \\ \frac{\xi}{\zeta^2}\widetilde{b} + \widetilde{\beta} & \Gamma_p,\ \Gamma_q \text{ have a common vertex or edge.} \end{cases}$$

The double layer kernel of the heat equation is the product of this term with the single layer kernel. The effect of the additional factor is that the leading term in integral (24) is ξ^3/ζ^4 in the cases of the self panel and a common edge and ξ^4/ζ^4 in the case of a common vertex. Thus the Duffy transform (25) will result in regular integrals.

Stokeslet

We use the form of the time dependent Stokeslet which can be found in [9]

$$G_{kl}(\mathbf{r}, s) = \frac{1}{s^{\frac{3}{2}}}\left[\delta_{kl}\psi_1(|\boldsymbol{\rho}|) + \rho_k\rho_l\,\psi_2(|\boldsymbol{\rho}|)\right]$$

where $\mathbf{r} = \mathbf{x} - \mathbf{y}$, $s = t - \tau$, $\boldsymbol{\rho}$ is defined in (3), $k, l \in \{1, 2, 3\}$ and the functions ψ_1, ψ_2 are given by

$$\psi_1(\rho) = \frac{1}{\pi^{\frac{3}{2}}}\frac{1}{\rho^3}\left(\gamma\left(\tfrac{3}{2}, \rho^2\right) - \gamma\left(\tfrac{5}{2}, \rho^2\right)\right),$$

$$\psi_2(\rho) = \frac{1}{\pi^{\frac{3}{2}}}\frac{1}{\rho^5}\gamma\left(\tfrac{5}{2}, \rho^2\right).$$

Here $\gamma(\alpha, z)$ is the incomplete gamma function

$$\gamma(\alpha, z) = \int_0^z \zeta^{\alpha-1}e^{-\zeta}d\zeta, \quad \alpha > 0,$$

see e.g. [22]. For our purposes we need the following properties, which follow immediately from this definition,

$$\gamma(\alpha, z) = z^{\alpha}\gamma^{*}(\alpha, z),$$
$$\gamma(\alpha, z) \sim \Gamma(\alpha), \quad z \to \infty.$$

Here $\gamma^{*}(\alpha, z)$ is an entire function in z and $\Gamma(\alpha)$ is the Euler gamma function. From these properties it follows that the ψ-functions are smooth and that the Stokeslet satisfies Assumption 1 with $n = M = 3$. Therefore the transformations in the previous sections will result in regular integrals.

Stresslet

We now turn to the stresslet of the transient Stokes flow. It is given by

$$T_{ijk}(\mathbf{r}, s) = \frac{1}{s^2}\Big[\left(\delta_{jk}\rho_i + \delta_{ik}\rho_j\right)\psi_3\left(|\boldsymbol{\rho}|\right) + \delta_{ij}\rho_k\psi_4\left(|\boldsymbol{\rho}|\right) + \rho_i\rho_j\rho_k\psi_5\left(|\boldsymbol{\rho}|\right)\Big] \tag{33}$$

where the functions ψ_3, ψ_4 and ψ_5 are defined by

$$\begin{aligned}
\psi_3(\rho) &= \frac{1}{\pi^{\frac{3}{2}}}\frac{1}{\rho^5}\left(3\gamma\left(\tfrac{5}{2}, \rho^2\right) - 2\gamma\left(\tfrac{7}{2}, \rho^2\right)\right),\\
\psi_4(\rho) &= -\frac{2}{\pi^{\frac{3}{2}}}\frac{1}{\rho^5}\gamma\left(\tfrac{5}{2}, \rho^2\right),\\
\psi_5(\rho) &= \frac{4}{\pi^{\frac{3}{2}}}\frac{1}{\rho^7}\gamma\left(\tfrac{7}{2}, \rho^2\right),
\end{aligned} \tag{34}$$

see [9]. The double layer kernel is

$$K_{ik}(\mathbf{r}, s) = T_{ijk}(\mathbf{r}, s)n_j(\mathbf{y}) + \frac{1}{4\pi}\frac{r_i}{|\mathbf{r}|^3}n_k(\mathbf{y})\delta(s), \tag{35}$$

where the Einstein summation convention is used. The delta function implies that the double layer potential involves an additional surface integral.

The Stresslet and double layer kernel satisfy Assumption 1 with $n = 4$ and $M = 4$. Hence Theorem 1 can only be applied for $m \geq 2$. In the case of identical time intervals and identical panels the integrals I_a and I_b in (26) and (27) are still singular. Likewise, for the surface integral due to the second term in (35) the spatial transformations of Section 3 will give smooth integrands only when $m \geq 2$.

That this case creates difficulties is not a surprise because the singularity in the double layer kernel must be understood as Cauchy principal value, see [9]. In this paper it is shown that for a stationary surface the Galerkin influence coefficients become weakly singular in space after time integration. This follows from the explicit form of the antiderivatives of the functions

$$\partial_t^{-1}\gamma\left(\alpha, |\boldsymbol{\rho}|^2\right) = \frac{|\mathbf{r}|^2}{4}\Gamma(\alpha - 1) + t\,\widetilde{\gamma}(\alpha, |\boldsymbol{\rho}|^2),$$

where the time dependence is in $\boldsymbol{\rho}$ and

$$\widetilde{\gamma}(\alpha, |\boldsymbol{\rho}|^2) = \gamma(\alpha, |\boldsymbol{\rho}|^2) - |\boldsymbol{\rho}|^2\gamma(\alpha - 1, |\boldsymbol{\rho}|^2).$$

Then the time integrated stresslet is

$$\int_0^s T_{ijk}(\mathbf{r}, s')\,ds' = -\frac{1}{4\pi}\delta_{ij}\frac{r_k}{|\mathbf{r}|^3} + \frac{3}{4\pi}\frac{r_i r_j r_k}{|\mathbf{r}|^5} + \frac{1}{s}T^{\mathrm{w}}_{ijk}(\mathbf{r}, s), \tag{36}$$

where

$$T^{\mathrm{w}}_{ijk}(\mathbf{r}, s) = \Big[\left(\delta_{jk}\rho_i + \delta_{ik}\rho_j\right)\widetilde{\psi}_3\left(|\boldsymbol{\rho}|\right) + \delta_{ij}\rho_k\widetilde{\psi}_4\left(|\boldsymbol{\rho}|\right) + \rho_i\rho_j\rho_k\widetilde{\psi}_5\left(|\boldsymbol{\rho}|\right)\Big].$$

The functions $\widetilde{\psi}_3$, $\widetilde{\psi}_4$ and $\widetilde{\psi}_5$ are defined just as in (34) but with $\gamma(\alpha, \rho^2)$ replaced by $\widetilde{\gamma}(\alpha, \rho^2)$. The first term on the right hand side in (36) cancels the second term in (35). The other term in (36) is the stresslet of the steady Stokes and is weakly singular in space. The third term, $T^{\mathrm{w}}_{ijk}(\mathbf{r}, s)/s$, is weakly singular in space–time and satisfies the assumptions of Theorem 1 with $n = 2$ and $M = 3$.

Consider now the strongly singular integral for the double layer potential. That is, an integral of the form (4) where the function G is now K_{ik} of (35) and $p = q$ and $j = i$. We split this integral into two pieces

$$I^{w}_{p,p} = \int_0^{h_t}\int_0^t\int_\sigma\int_\sigma K_{ik}(\mathbf{x} - \mathbf{y}, t - \tau)\phi(\hat{\mathbf{x}}, t, \hat{\mathbf{y}}, \tau) - K_{ik}(\mathbf{x} - \mathbf{y}', t - \tau)\phi(\hat{\mathbf{x}}, t, \hat{\mathbf{y}}, t)\,d\hat{\mathbf{y}}d\hat{\mathbf{x}}d\tau dt,$$

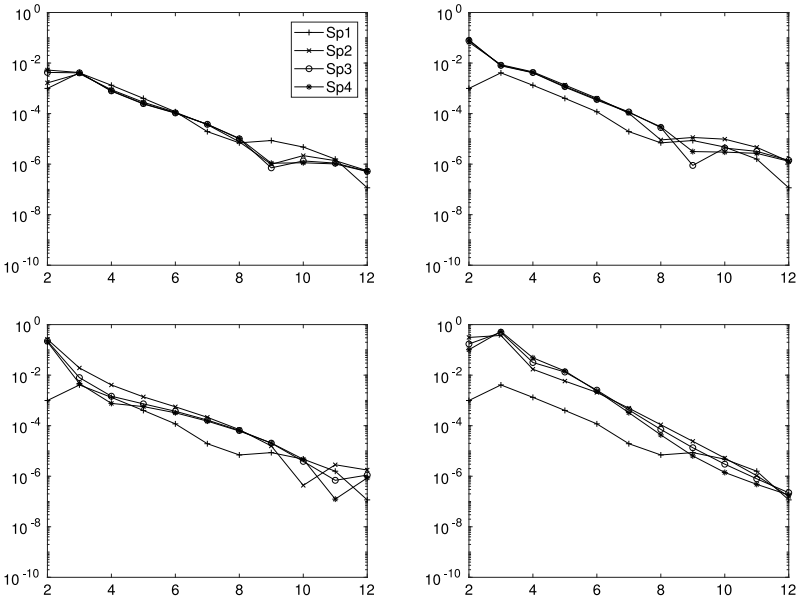

Fig. 4. Cubature errors versus order for $I_j = I_i$, top left to bottom right: Self panel, common edge, common vertex and separated panels.

and

$$I^s_{p,p} = \int_0^{h_t} \int_\sigma \int_\sigma \int_0^t K_{ik}(\mathbf{x} - \mathbf{y}', t - \tau)\, d\tau\, \phi(\hat{\mathbf{x}}, t, \hat{\mathbf{y}}, t)\, d\hat{\mathbf{y}} d\hat{\mathbf{x}} dt.$$

where $\mathbf{x} = \mathbf{x}_p(\hat{\mathbf{x}}, t)$, $\mathbf{y} = \mathbf{x}_p(\hat{\mathbf{y}}, \tau)$ and $\mathbf{y}' = \mathbf{x}_p(\hat{\mathbf{y}}, t)$. That is, the primed quantities are evaluated at t instead of τ.

For the first integral we have from Lemma 1 and (7) that

$$\boldsymbol{\rho} - \boldsymbol{\rho}' = \mathbf{b}(\hat{\mathbf{x}}, \hat{\mathbf{y}}, t, \tau)(\hat{\mathbf{x}} - \hat{\mathbf{y}})\sqrt{t - \tau},$$

where $\mathbf{b}$ is a smooth function. Since the functions in (34) are analytic, the factor $\sqrt{t - \tau}$ contributes an additional factor of ζ in (24). Thus we get $n = 3$ in Theorem 1 and therefore $I^w_{p,p}$ has a smooth integrand in the transformed coordinates.

In integral $I^s_{p,p}$ the τ integration gives the time integrated stresslet. Since the $r_k/|\mathbf{r}|$ part cancels, it remains to compute a surface integral for the stresslet of the steady Stokes kernel and an integral with $T^{\mathrm{w}}_{ijk}(\mathbf{r}, t)$. The former is smooth in the transformed spatial coordinates. For the latter the spatial transformations and the temporal transformation $t = h_t \zeta^2$ result in an integral of the form

$$I^w_{p,p} = \int_0^1 \int_0^1 \int_{[0,1]^3} \widetilde{T}^{\mathrm{w}}_{ijk}\left(\frac{\xi}{\zeta} A\mathbf{r}, \xi, \zeta, \boldsymbol{\eta}\right) d^3\boldsymbol{\eta}\, d\xi\, d\zeta.$$

Proceeding as before, with the Duffy transform (25) leads to an integral with a smooth integrand.

7. Numerical examples

To illustrate how the singularity removing transformations work with standard cubature methods we present results obtained with tensor product Gauss–Legendre rules. In this example we consider piecewise constant elements in space and time for the single layer potential of the heat equation on a translating unit sphere $\Gamma(t) = \mathbb{S} + \mathbf{e}_1 \sin(2\pi t)$. The triangulation of $\mathbb{S}$ is obtained by radial projection of uniform subdivisions of the unit cube. It is well known that for optimal convergence the time step size and the spatial meshwidth must scale like $h_t \sim h_s^2$, see [5,10], therefore we first consider space time refinements starting with 192 panels and $h_t = 0.025$ (Sp1), 768 panels and $h_t = 0.00625$ (Sp2), and so on. Figs. 4 and 5 display the relative cubature errors for different singular and non-singular cases and four mesh refinements. Since no analytical values are available, we have computed the integrals to very high order until convergence occurred in the first twelve significant digits. These values were used instead of the exact value for the error of the lower order calculations.

It is well known that the convergence of Gauss quadrature is exponential in the order if the integrand is analytic. However, it should be noted that (26) is 'only' smooth. Nevertheless, in the figures the convergence appears to be close to exponential. Moreover, the convergence is relatively unaffected by the meshsize if optimal space–time scaling is maintained. On the other hand, Fig. 6 displays errors for a fixed spatial mesh while the time step size is decreased. Here one can see that the convergence rate decreases with larger h_t.

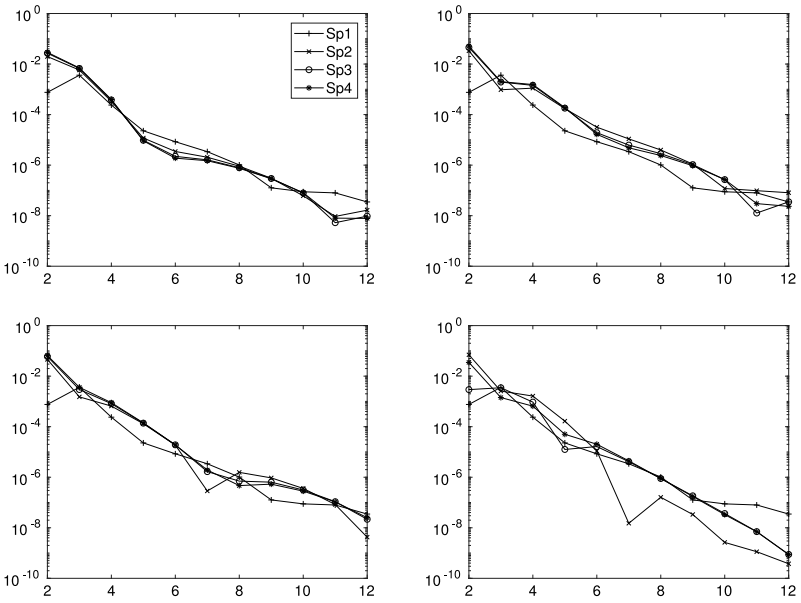

Fig. 5. Cubature errors versus order for $I_j = I_{i-1}$, top left to bottom right: Self panel, common edge, common vertex and separated panels.

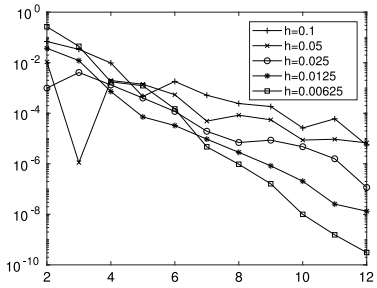

Fig. 6. Cubature errors versus order for refining the time stepsize. $I_j = I_i$, Self panel.

We have also implemented the quadrature method to solve the two-dimensional heat equation. The smaller dimensionality allows us to calculate more mesh refinements to fully investigate the convergence behavior of a fully discrete Galerkin method. We consider a time dependent curve that is broken up into segments $\Gamma_p(t)$, which are parameterized as $\mathbf{x} = \mathbf{x}_p(\hat{x}, t)$ where $\hat{x} \in [0, 1]$. Singularities occur when two segments are either identical or have a common end point. These can be treated by transforms similar to those described in Section 3. Since this is a straight forward application of this methodology we omit the details here, we only mention that after the time transforms of Section 4 one obtains integrals of the form (24) with the only difference that the variable $\boldsymbol{\eta}$ has now two instead of four components. Then the remainder of Section 5 implies that we obtain smooth integrands.

The weakly singular boundary integral equation for the heat equation exterior to the domain $\Omega(t)$ is

$$\int_0^t \int_{\Gamma(\tau)} G(\mathbf{x}, \mathbf{y}, t-\tau) \frac{\partial u}{\partial n}(\mathbf{y}, \tau)\, ds(\mathbf{y}) d\tau =$$
$$\tfrac{1}{2} u(\mathbf{x}, t) + \int_0^t \int_{\Gamma(\tau)} \left(\frac{\partial G}{\partial n}(\mathbf{x}, \mathbf{y}, t-\tau) - G(\mathbf{x}, \mathbf{y}, t-\tau) v_n \right) u(\mathbf{y}, \tau)\, ds(\mathbf{y}) d\tau .$$

Here, the normal velocity of the surface $v_n = v_n(\mathbf{y}, \tau)$ appears as an additional term for time dependent surfaces, see e.g. [15]. For the solution of the heat equation $u(x, t) = G(x - x_0, t)$ where x_0 is a point inside the domain $\Omega(0)$ we solve the Dirichlet problem for the known Neumann data, where the ansatz and test space consist of the piecewise constants in space and time. Furthermore, the Dirichlet data are replaced by their piecewise linear/constant interpolation in space/time. We have tested two geometries, a unit square that rotates in the time interval $[0, 1]$ once about its center and a translating unit circle whose center has time dependent coordinates $x_0(t) = 2\cos(2\pi t) - 2$ and $y_0(t) = 2\sin(2\pi t)$. We use tensor-product Gauss–Legendre quadrature to compute the transformed integrals. Thus the error of the solution depends on the mesh width in

Table 1
L_2 errors of the Galerkin solution, N_s and N_t are the number of spatial and temporal nodes. Rotating Square.

N_s	N_t			
	20	80	320	1280
10	0.57371	0.53451	0.55592	0.56598
20	0.48216	0.31812	0.31938	0.32498
40	0.53286	0.18653	0.16466	0.16906
80	16.7322	0.20098	0.08928	0.08544
160	3.7e+33	0.44416	0.10549	0.04709

Table 2
L_2 errors of the Galerkin solution. Translating Circle.

N_s	N_t			
	20	80	320	1280
10	0.97917	0.78284	0.70532	0.62064
20	0.91415	0.34885	0.34608	0.30676
40	0.97190	0.47609	0.10426	0.15189
80	13.9612	0.59329	0.17262	0.04972
160	4.2e+21	0.51388	0.24019	0.07202

Table 3
L_2 errors of the Galerkin solution for increasing quadrature order. $N_t = 20$, rotating square.

p	$N_s = 20$	$N_s = 80$
p = 6	0.5737110	16.7322237
p = 10	0.5734032	4.5891282
p = 14	0.5734124	2.9760603
p = 18	0.5734102	2.5127979
p = 22	0.5734091	2.3483674
p = 26	0.5734096	2.2906505
p = 30	0.5734097	2.2742646

space and time as well as the quadrature order. Tables 1 and 2 show the errors for mesh refinements and a fixed quadrature order of six.

We see that the theoretical $O(\sqrt{h_t} + h_s)$ behavior is well reproduced near the diagonals of the table. It is also apparent that errors in the lower left corners of the table become larger.

This is not a discretization but a cubature error. As already seen in Fig. 6 this error increases when h_t becomes large in comparison with the panel size. We recompute the entries $(N_s, N_t) = (10, 20)$ and $(N_s, N_t) = (80, 20)$ of Table 3 for different quadrature orders.

The results can be interpreted as follows. In column $N_t = 20$ the mesh ratio is sufficiently large and the shown L_2-errors of the discretized solution show very little dependence on the quadrature order. Column $N_t = 80$ corresponds to a small mesh ratio and exhibits a strong dependence. Fortunately, near the optimal mesh ratio the cubature converges rapidly.

References

[1] G.F. Dargush, P.K. Banerjee, Application of the boundary element method to transient heat conduction, Internat. J. Numer. Methods Engrg. 31 (1991) 1231–1247.
[2] M.M. Grigoriev, G.F. Dargush, Higher-order boundary element methods for transient diffusion problems. part I: Bounded flux formulation, Internat. J. Numer. Methods Engrg. 55 (2002) 1–40.
[3] C.C. Tsai, D.L. Young, C.M. Fan, C.W. Chen, MFS with time-dependent fundamental solutions for unsteady Stokes equations, Eng. Anal. Boundary Elem. 30 (2006) 897908.
[4] E.A. McIntyre, Boundary integral solutions of the heat equation, Math. Comp. 46 (173) (1986) 71–79.
[5] M. Costabel, Boundary integral operators for the heat equation, Integral Equations Operator Theory 13 (4) (1990) 498–552.
[6] G.C. Hsiao, W.L. Wendland, Boundary Integral Equations, in: Applied Mathematical Sciences, vol. 168, Springer, 2008.
[7] C. Bacuta, M.E. Hassell, G.C. Hsiao, F.-J. Sayas, Boundary integral solvers for an evolutionary exterior Stokes problem, SIAM J. Numer. Anal. 53 (3) (2015) 1370–1392.
[8] M. Costabel, Time-dependent problems with the boundary integral equation method, in: E. Stein, R. de Borst, T. Hughes (Eds.), Encyclopedia of Computational Mathematics, Wiley, 2004.
[9] Y.O. Choi, J. Tausch, The Galerkin boundary element method for transient Stokes flow, Adv. Comput. Math. 43 (3) (2017) 473–493.
[10] P.J. Noon, The Single Layer Heat Potential and Galerkin Boundary Element Methods for the Heat Equation (Ph.D. thesis), University of Maryland, 1988.
[11] S. Erichsen, S.A. Sauter, Efficient automatic quadrature in 3-D Galerkin BEM, Comput. Methods Appl. Mech. Eng. 157 (1998) 215–224.
[12] S. Sauter, C. Schwab, Randelementmethoden: Analyse, Numerik Und Implementierung Schneller Algorithmen, Teubner, Stuttgart, 2004.
[13] M. Messner, M. Schanz, J. Tausch, Fast Galerkin method for parabolic space–time boundary integral equations, J. Comput. Phys. 258 (1) (2014) 15–30.

[14] M. Messner, M. Schanz, J. Tausch, An efficient Galerkin boundary element method for the transient heat equation, SIAM J. Sci. Comput. 258 (1) (2015) A1554–A1576.
[15] K. Brattkus, D. Meiron, Numerical simulations of unsteady crystal growth, SIAM J. Appl. Math. 52 (1992) 1303–1320.
[16] J.A. Sethian, J. Strain, Crystal growth and dendritic solidification, J. Comput. Phys. 98 (2) (1992) 231–253.
[17] X. Wang, J. Kanapka, W. Ye, N.R. Aluru, J. White, Algorithms in faststokes and its application to micromachined device simulation, IEEE Trans. CAD 25 (2) (2005) 248–257.
[18] A. Farutin, Amoeboid swimming: A generic self-propulsion of cells in fluids by means of memebrane deformation, Phys. Rev. Lett. 111 (2013).
[19] K. Gustavsson, A.-K. Tornberg, Gravity induced sedimentation of slender fibers, Phys. Fluids 21 (1) (2009) 123301.
[20] A. Chernov, C. Schwab, Exponential convergence of Gauss-Jacobi quadratures for singular integrals over simplices in arbitrary dimension, SIAM J. Numer. Anal. 50 (3) (2012) 1433–1455.
[21] A. Chernov, A. Reinarz, Numerical quadrature for high-dimensional singular integrals over parallelotopes, Comput. Math. Appl. 66 (7) (2013) 1213–1231.
[22] F.W.J. Olver, D.W. Lozier, R.F. Boisvert, C.W. Clark (Eds). NIST Handbook of Mathematical Functions, Cambridge, 2010.